Chemistry–A European Journal

Supporting Information

Stable Triarylmethyl Radicals and Cobalt(II) Ions Based 1D/2D Coordination Polymers

Xudong Hou, Giang Truong Nguyen, Tingting Xu, Haipeng Wei, Tun Seng Herng, Guifei Huo, Dingguan Wang, Jun Ding, Shaofei Wu,* Liviu Ungur,* and Jishan Wu*

Table of contents

1. Experimental session

1.1 General

All reagents and starting materials were obtained from commercial suppliers and used without further purification unless otherwise noted. Anhydrous tetrahydrofuran (THF) was distilled from sodium-benzophenone immediately prior to use. Anhydrous dichloromethane (DCM) was distilled from CaH_2. All reaction conditions dealing with air and moisture-sensitive compounds were carried out in a dry reaction vessel under a N_2 atmosphere. Compound **TTM** was synthesized according to the literature.[1] The ^1H NMR and ^{13}C NMR spectra were recorded in the solution of $CDCl_3$ and CD_2Cl_2 on Bruker AVANCE (500 MHz) spectrometer. All chemical shifts are quoted in ppm, with tetramethylsilane (TMS) as the internal standard. The following abbreviations were used to explain the multiplicities: s = singlet, d = doublet, t = triplet, m = multiplet. High-resolution electrospray ionization (ESI) mass spectra were recorded on a MicrOTOFQII instrument. UV-vis-NIR absorption spectra were recorded on a Shimadzu UV-3600 spectrophotometer. Inductively coupled plasma−optical emission spectrometry (ICP-OES) experiments were carried out on a Perkin Elmer Avio 500 Inductively Coupled Plasma-Optical Emission Spectrometer (ICP-OES). Elemental microanalyses (EA) were performed in the Thermo Fisher Scientific Flash Smart CHNS Elemental Analyser. Single crystals were measured at low temperature (T = 100 K) on a four circles goniometer Kappa geometry Bruker AXS D8 Venture equipped with a Photon 100 CMOS active pixel sensor detector using a Molybdene monochromatized (λ = 0.71073Å) or using a Copper monochromatized (λ = 1.54178 Å) X-Ray radiation. Continuous wave X-band ESR spectra were obtained with a JEOL (FA200) spectrometer using a variable temperature liquid nitrogen cryostat. A Quantum Design 7 Tesla SQUID-VSM system was available for the magnetic measurement of the freshly prepared **CoCP-1** and **CoCP-2** in this work. The crystalline samples with a weight of 5-10 mg were sealed in a plastic capsule. Magnetic moment was measured in the temperature range of 2 to 300 K. The empty plastic capsule exhibited diamagnetic and its magnetic moment was measured for correction. The diamagnetic contribution from the samples was estimated according to a reported method[2] and the component was also subtracted from the recorded magnetic moment. Powder X-ray diffraction (PXRD) data were recorded on a Bruker D8 Advance Powder X-ray Diffractometer by depositing powder on the sample cell with the angle 2θ varied from 5° up to 30° at a 0.02° increment. XPS measurements were performed on a VG Scienta-R4000 spectrometer using a using Mg Ka X-ray (1253.6 eV) source. A conductive Cu tape was attached to the holder and the sample power was pressed on the Cu tape to form a thin organic layer. All photoemission spectra were collected at an emission angle of 90° with respect to the sample surface and operated in an ultrahigh vacuum (UHV) chamber with a base pressure of 1×10^{-9} mbar.

1.2. Synthetic procedures and characterization data

Synthesis of the radical ligands **L1** and **L2**

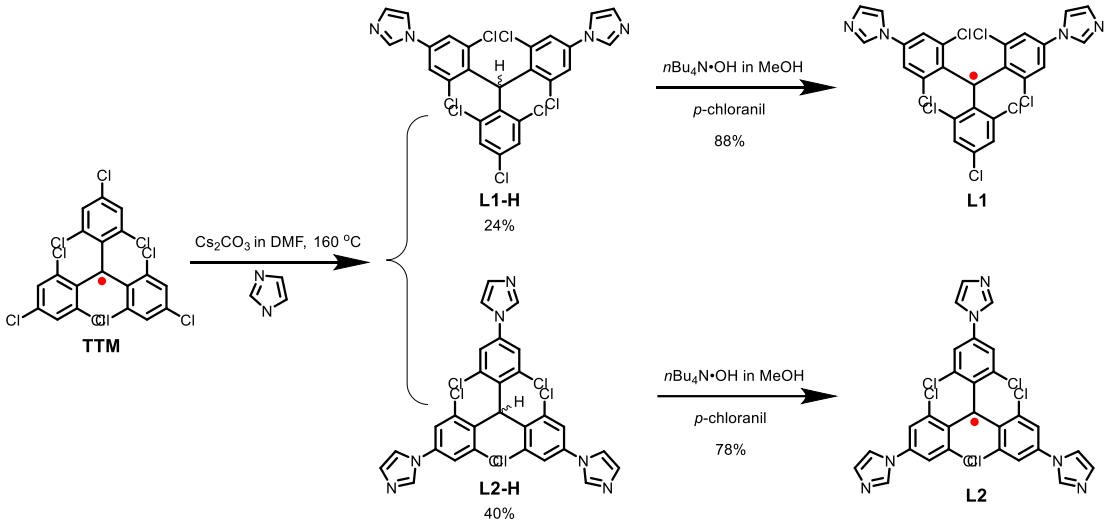

A mixture of TTM (1.32 g, 2.38 mmol), imidazole (1.30 g, 19.04 mmol), anhydrous Cs_2CO_3 (0.88 g, 2.62 mmol) and DMF (50 mL) was stirred at 160 °C for 18 h under argon atmosphere and dark conditions. After cooling down to room temperature, the reaction mixture was poured into hydrochloric acid solution (0.1 M). The precipitate was filtered and washed with water for three times. The crude product was dissolved in dichloromethane and extracted with water and dichloromethane. The organic layer was dried over Na_2SO_4 and the solvent was removed by rotary evaporator under vacuum. The crude product was purified by silica gel column chromatography using a mixture of dichloromethane and ethyl acetate as the eluent to give mainly hydrogenated precursors **L1-H** and **L2-H**.

L1-H: Light red powder (0.35 g, 24%); ^{1}H NMR (500 MHz, CD_2Cl_2): δ ppm 7.90 (s, 2H), 7.49 (dd, J = 1.1, 2.4 Hz, 2H), 7.44 (d, J = 2.3 Hz, 1H), 7.36 (dd, J = 2.3, 3.5 Hz, 2H), 7.32 (s, 2H), 7.31 (s, 1H), 7.19 (s, 2H), 6.83 (s, 1H); HRMS analysis (APCI): calcd for $C_{25}H_{14}Cl_7N_2$ $(M+H)^+$: 614.9033, found: 614.9038 (error: 0.81 ppm).

L2-H: Light red powder (0.55 g, 40%); ^{1}H NMR (500 MHz, CD_2Cl_2): δ ppm 7.90 (s, 3H), 7.51 (d, J = 2.4 Hz, 3H), 7.38 (d, J = 2.4 Hz, 3H), 7.34 (t, J = 1.3 Hz, 3H), 7.20 (s, 3H), 6.90 (s, 1H), HRMS analysis (APCI): calcd for $C_{28}H_{17}Cl_6N_6$: 646.9640, found: 646.9644 (error: 0.62 ppm).

Under argon atmosphere and dark conditions, the tetra-*n*-butylammonium hydroxide (3.0 eq.) was added to **L1-H** or **L2-H** (1.0 eq.) in dry THF and the solution acquired a light red color. The solution was stirred for 5 h at room temperature. Then p-chloranil (5.0 eq.) was added, and the solution was stirred for a further 2 h. The solvent was removed under vacuum, and the crude product was purified by silica gel column chromatography using the mixture of dichloromethane and ethyl acetate as the eluent to give the radical ligands **L1** and **L2** in 88% and 78% yield, respectively.

L1: Deep red powder; APCI (*m*/*z*): $[M+H]^+$ Calcd for $C_{25}H_{13}Cl_7N_4$, 613.8954; Found, 613.8959. Elem. Anal. Calcd for $C_{25}H_{12}Cl_7N_4$, C 48.7, H 1.96, N 9.09; Found, C 50.27, H 2.31, N 9.80.

L2: Deep red powder; APCI (*m*/*z*): [M] Calcd for $C_{28}H_{16}Cl_6N_6$, 645.9571; Found, 645.9562 (error: 1.39 ppm). Elem. Anal. Calcd for $C_{28}H_{16}Cl_6N_6$, C 51.81, H 2.48, N 12.95; Found, C 52.29, H 2.31, N 11.80.

Synthesis of the **CoCP-1** and **CoCP-2**

For **CoCP-1**: A solution of **L1** (6.13 mg, 0.01 mmol) in dimethylformamide (10 mL) was added to the bottom of a straight glass tube, followed by the layering of EtOH /dimethylformamide mixture

solvents. Then a solution of $CoCl_2$ (1.3 mg, 0.01 mmol) in EtOH (10 mL) was carefully layered on the top and dark red single crystals were obtained after 1-2 weeks. The crystals were collected and washed with EtOH and dimethylformamide. The activated sample (2.96 mg) was obtained in 46% yield under vacuum for 24 h. Elemental analysis: calcd. (%) for $C_{56}H_{38}Cl_{16}CoN_{10}O_2$: C 44.57, H 2.54, N 9.28; found: C 43.91, H 2.06, N 9.18. ICP-OES calcd. (%) for $C_{56}H_{38}Cl_{16}CoN_{10}O_2$: Co = 3.91; found: Co =3.87.

For **CoCP-2**: A solution of **L2** (6.46 mg, 0.01 mmol) in dimethylformamide (10 mL) was added to the bottom of a straight glass tube, followed by the layering of EtOH / dimethylformamide mixture solvent. Then a solution of $Co(NTf)_2$ (12.38 mg, 0.02 mmol) in EtOH (10 mL) was carefully layered on the top, and dark red single crystals were obtained after 1-2 weeks. The crystals were collected and washed with EtOH and dimethylformamide. The activated sample (2.96 mg) was obtained in 41% yield under vacuum for 24 h. Elemental analysis: calcd. (%) for $C_{78}H_{72}Cl_{12}CoF_{12}N_{20}O_{14}S_4$: C 39.8, H 3.08, N 11.90; found: C 40.62, H 3.01, N 10.78. ICP-OES calcd. (%) for $C_{78}H_{72}Cl_{12}CoF_{12}N_{20}O_{14}S_4$: Co = 2.50; found: Co =2.48.

1.3. Additional spectra

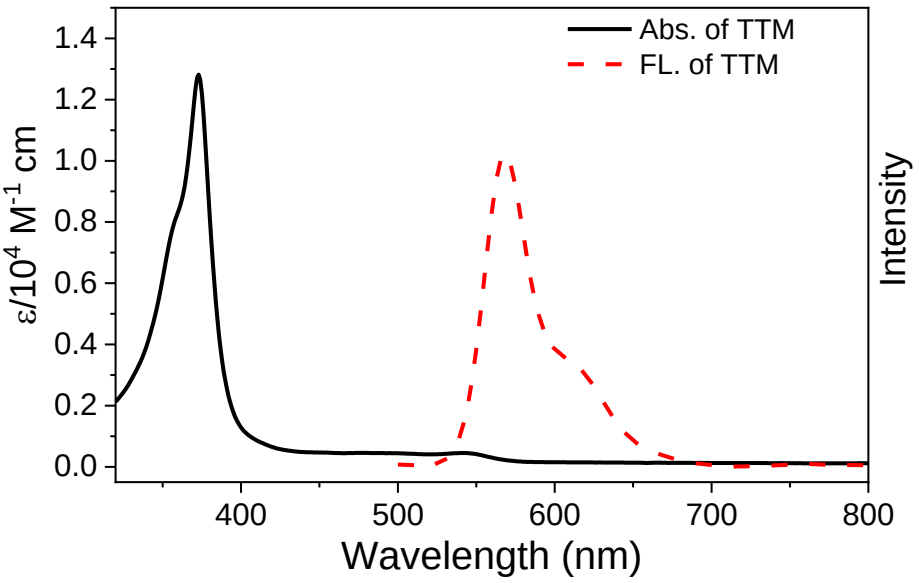

Figure S1. UV−vis absorption (abs) and normalized fluorescence (FL) spectra of **TTM** measured in DCM. The excitation wavelength is 373 nm.

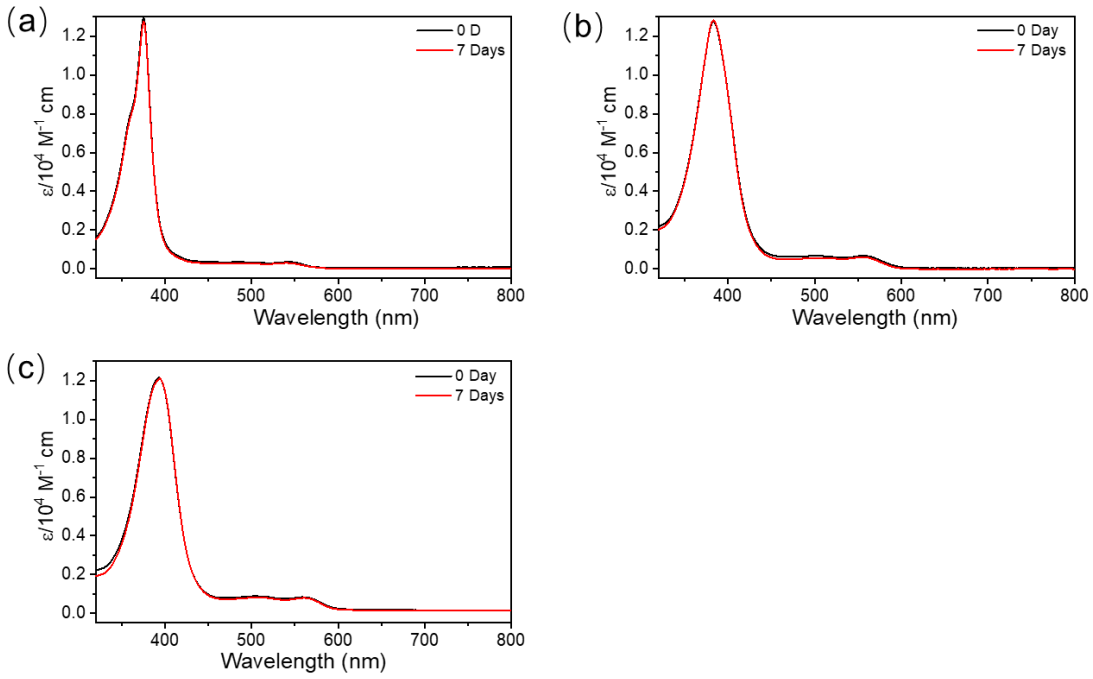

Figure S2. Time-dependent UV-vis absorption spectra of **TTM** (a), **L1** (b) and **L2** (c) in DCM (1×10^{-4} M) measured in the air under dark conditions. No obvious absorption spectral change was observed after 7 days.

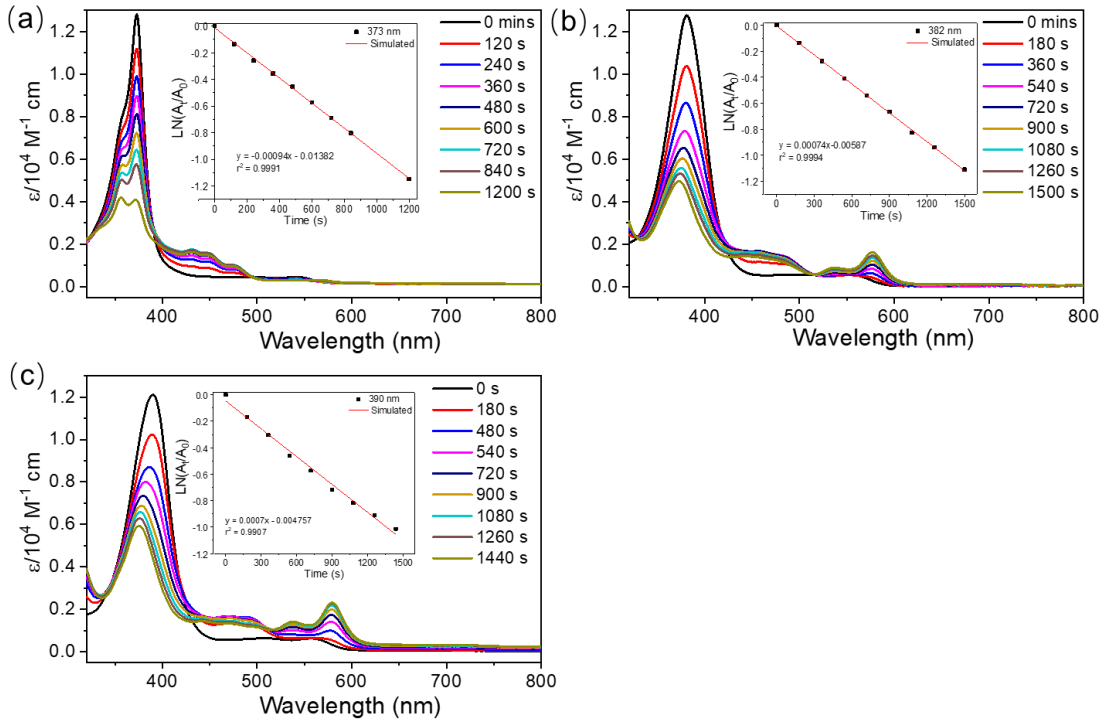

Figure S3. Time dependent UV-vis absorption spectra of **TTM** (a), **L1** (b) and **L2** (c) in DCM (1×10^{-4} M) measured under air and ambient light conditions. Inset are the pseudo- first-order kinetics of the degradation when monitored at 373, 380 and 392 nm, respectively, and the half-life times were estimated to be 723 (**TTM**), 922 (**L1**) and 983 s (**L2**), respectively.

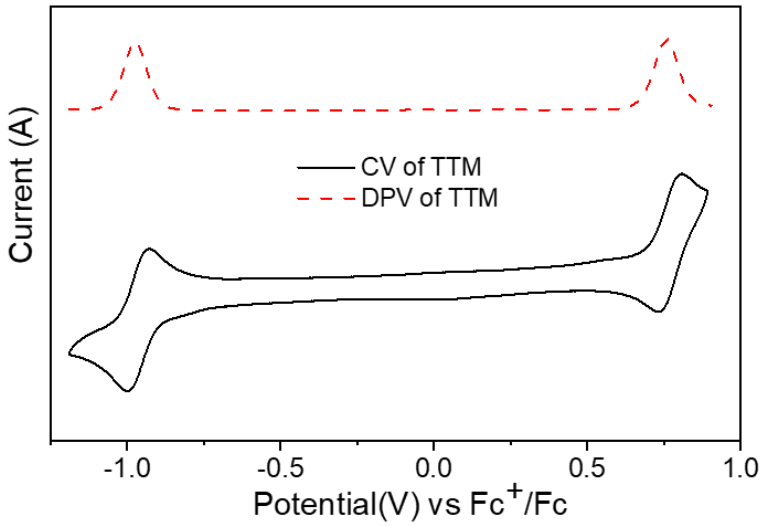

Figure S4. Cyclic voltammogram (CV) and differential pulse voltammogram (DPV) of **TTM** in DCM (V vs Fc/Fc^{+}), with 0.1 M $n$$Bu_4NPF_6$ as supporting electrolyte and scan rate: 100 mV/s for CV.

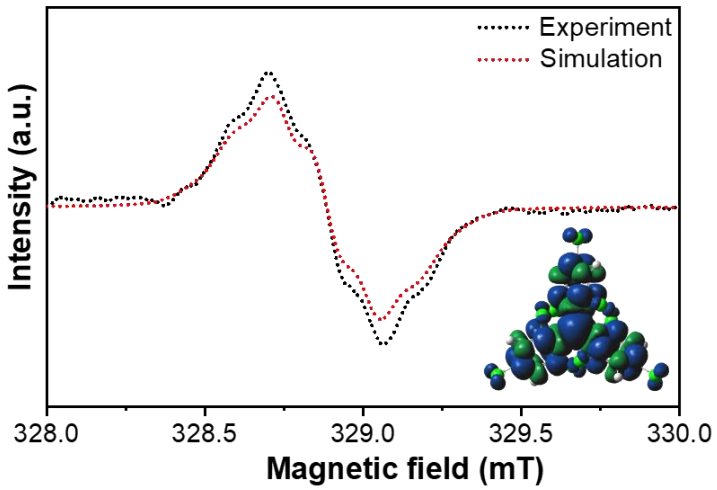

Figure S5. ESR spectrum of **TTM** in DCM at RT and simulated ESR spectrum. Inset is the calculated spin-density-distribution map for the **TTM**.

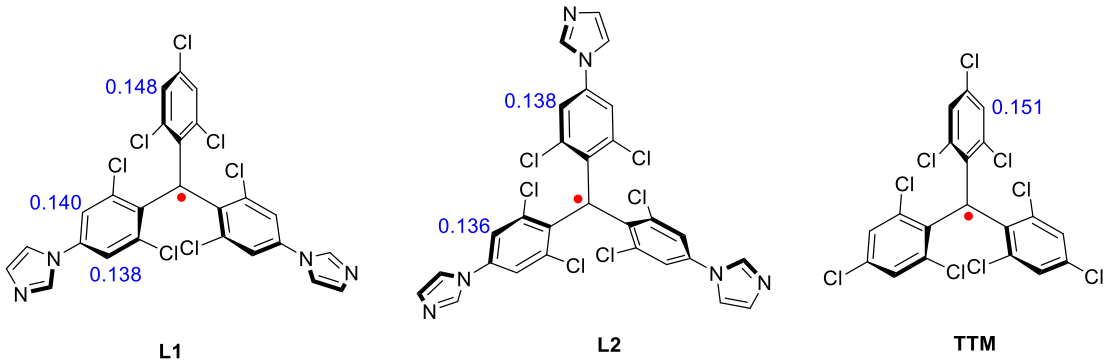

Figure S6. Hyperfine coupling constants (blue numbers, in mT) used for the simulation of the ESR spectra of **TTM**, **L1** and **L2**.

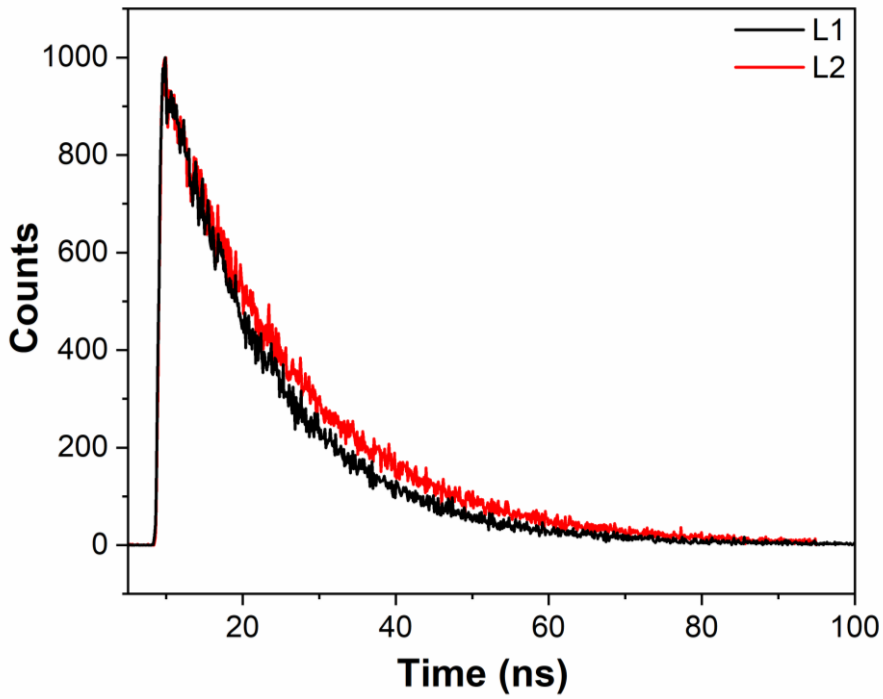

Figure S7. Transient photoluminescence decay spectra of **L1** (black), **L2 (**red) in DCM (10^{-5} M) at room temperature

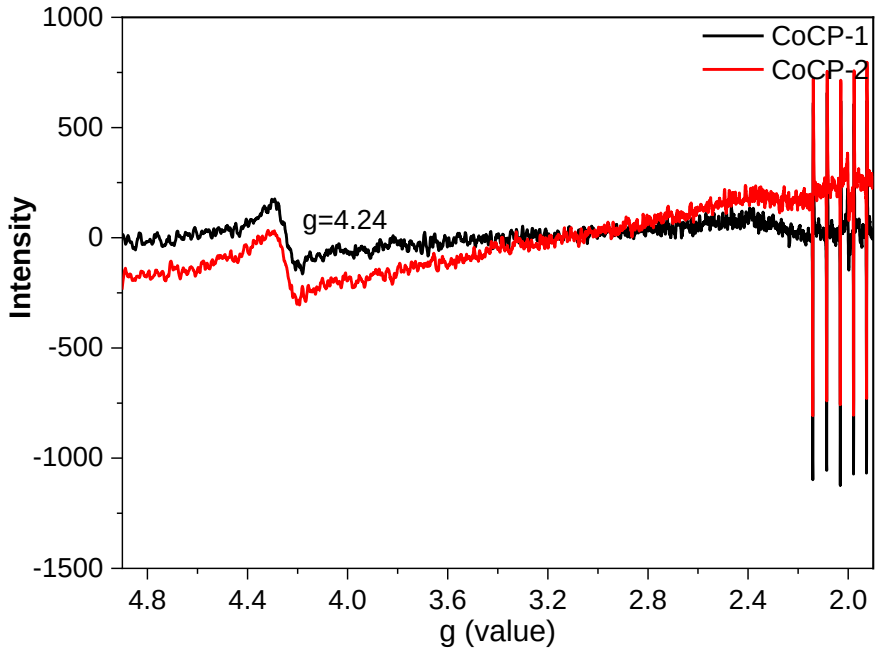

Figure S8. Full-range ESR spectra of **CoCP-1** and **CoCP-2** measured at room temperature.

2. Theoretical calculations

2.1. Time-dependent DFT (TD-DFT) calculations of the organic radical ligands

TD DFT calculations were performed at the UB3LYP/6-31G(d,p) level of theory under vacuum using Gaussian 09 package.[3]

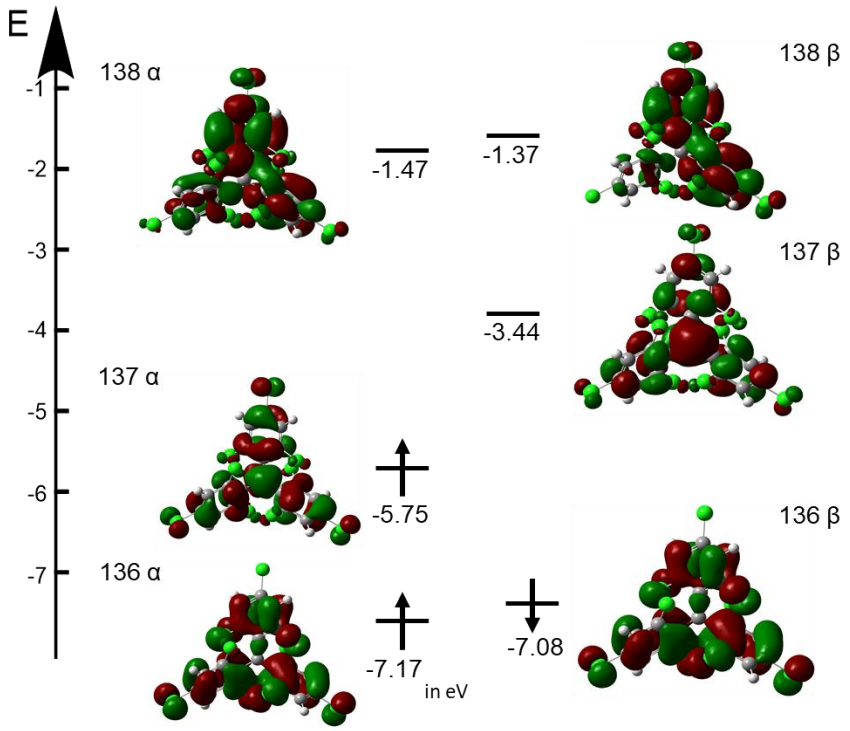

Figure S9. Frontier molecular orbital profiles and energy diagram (in eV) of **TTM** obtained by UB3LYP/6-31G(d,p) level calculation.

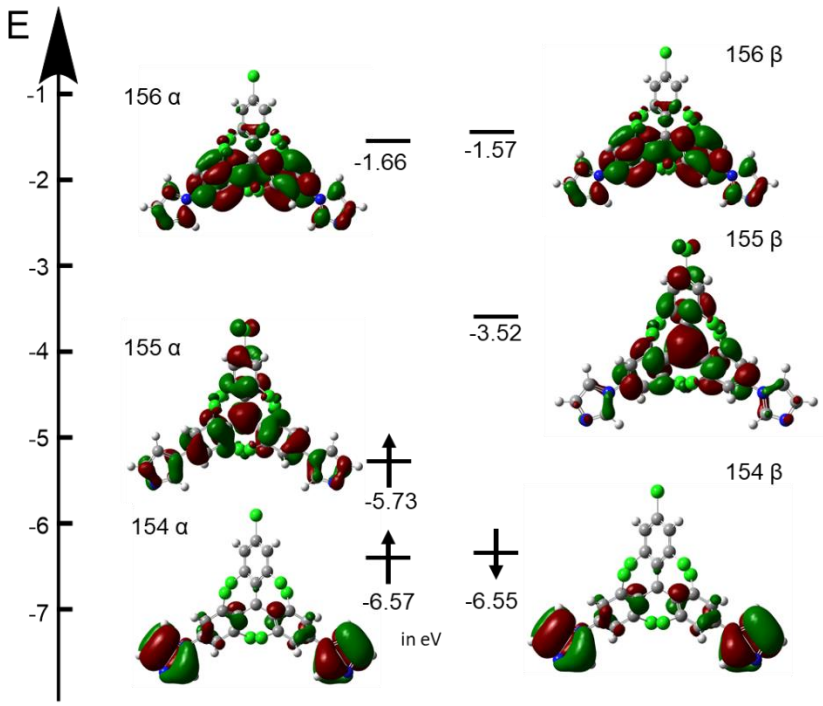

Figure S10. Frontier molecular orbital profiles and energy diagram (in eV) of **L1** obtained by UB3LYP/6-31G(d,p) level calculation.

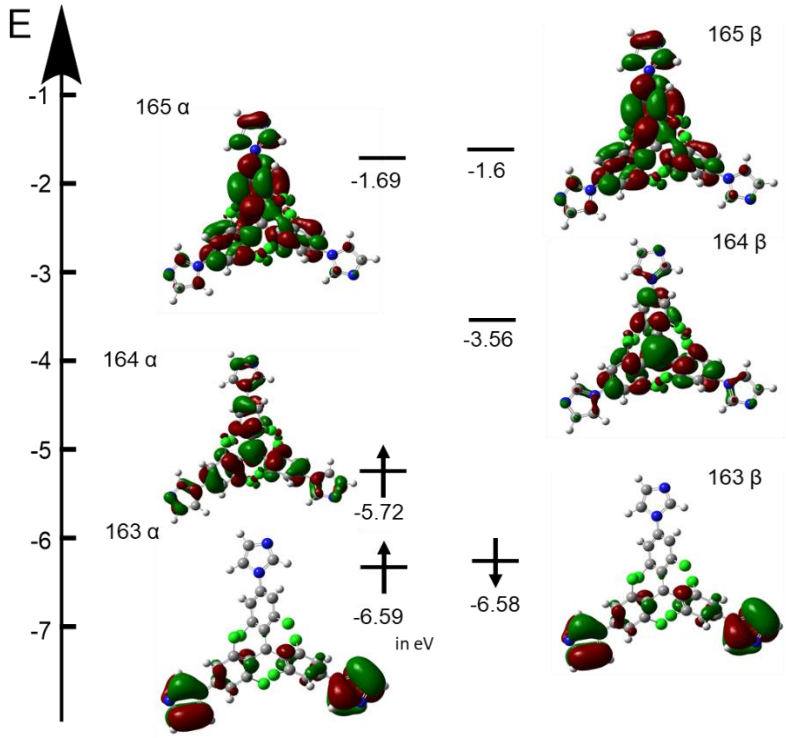

Figure S11. Frontier molecular orbital profiles and energy diagram (in eV) of **L2** obtained by UB3LYP/6-31G(d,p) level calculation.

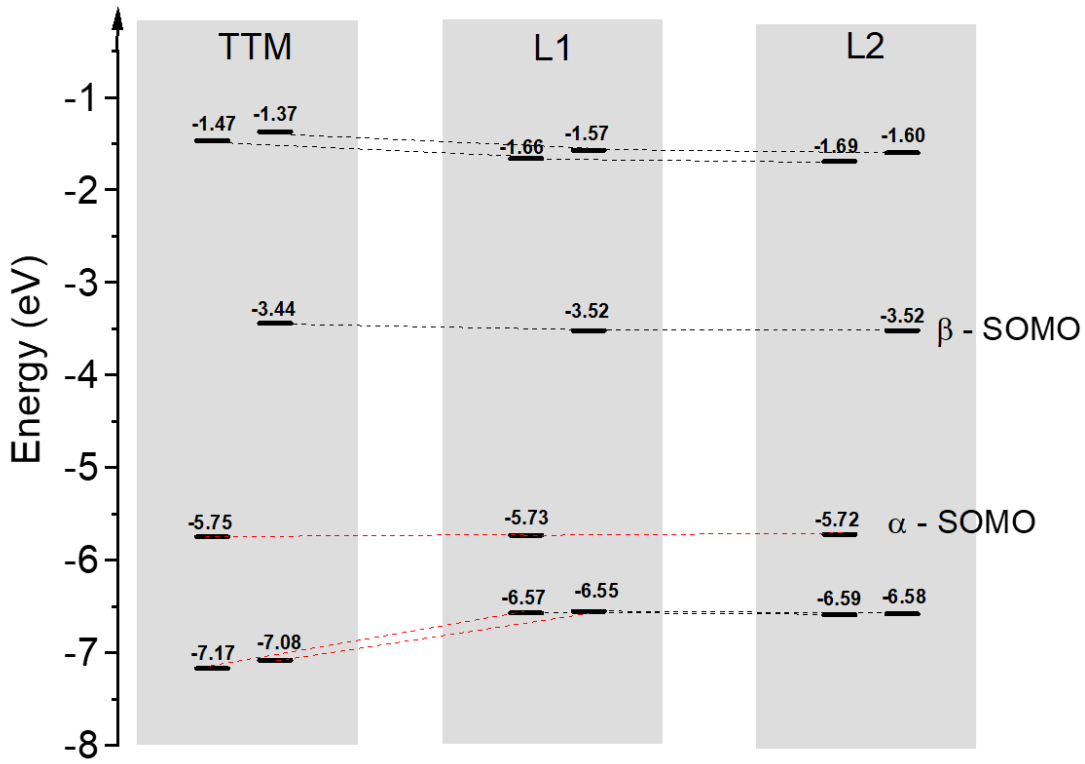

Figure S12. Summary of energy diagram (in eV) of the radicals calculated by DFT (UB3LYP/6-31G(d,p)).

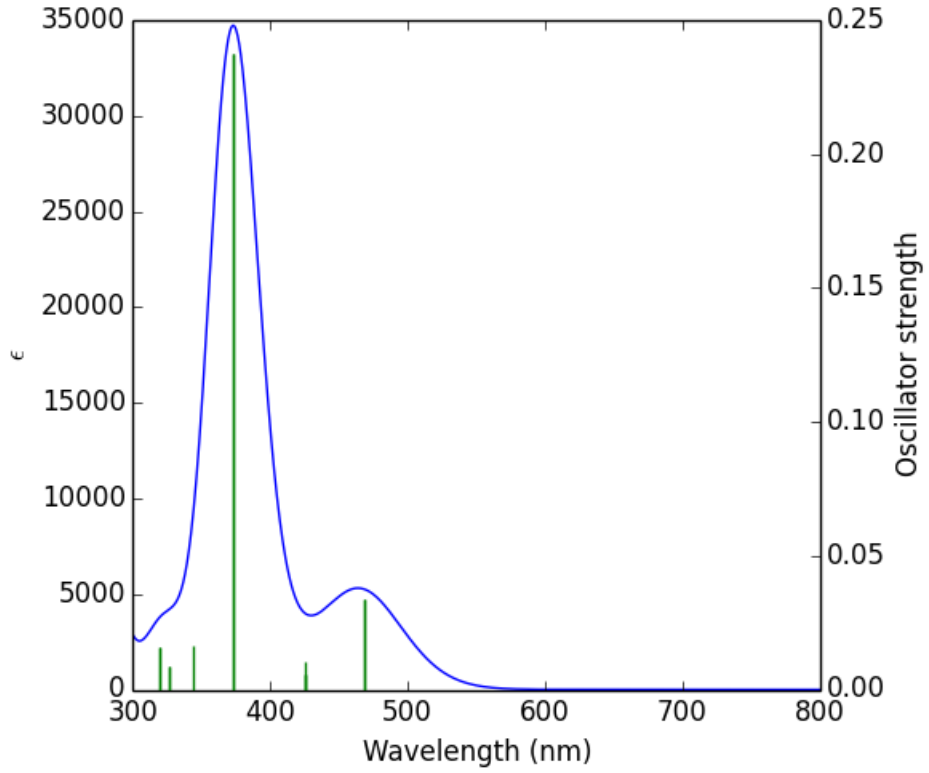

Figure S13. Calculated electronic absorption spectrum (UB3LYP/6-31G(d,p)) of **TTM**.

Table S1. Selected TD-DFT (UB3LYP/6-31G(d,p)) calculated energies, oscillator strength and compositions of major electronic transitions of **TTM**.

Wavelength (nm)	Osc. Strength	Symmetry	Major contribs
468.4482299	0.0337	2.205-A	H-1(β)->LUMO(β) (47%), HOMO(β)->LUMO(β) (32%)
468.3951379	0.0335	2.205-A	H-1(β)->LUMO(β) (32%), HOMO(β)->LUMO(β) (47%)
425.799138	0.0102	2.098-A	H-2(β)->LUMO(β) (89%)
425.5068742	0.0056	2.122-A	H-4(β)->LUMO(β) (81%)
425.4776699	0.0059	2.120-A	H-3(β)->LUMO(β) (76%)
402.1674171	0	2.345-A	H-5(β)->LUMO(β) (77%)
373.3676424	0.2374	2.369-A	HOMO(α)->LUMO(α) (65%)
373.3339145	0.2375	2.369-A	HOMO(α)->L+1(α) (65%)
343.8942474	0.0164	2.208-A	HOMO(α)->L+2(α) (92%)
336.3104026	0	3.257-A	H-3(A)->L+2(A) (10%), H-5(β)->LUMO(β) (16%)
326.833249	0.0089	2.352-A	HOMO(α)->L+3(α) (81%)
326.7901766	0.0088	2.352-A	HOMO(α)->L+4(α) (81%)
319.3658055	0.0157	3.151-A	H-4(A)->L+2(α) (7%), H-3(α)->L+4(α) (9%),
319.3329032	0.0157	3.152-A	HOMO(α)->LUMO(α) (7%), HOMO(α)->L+1(α) (9%),

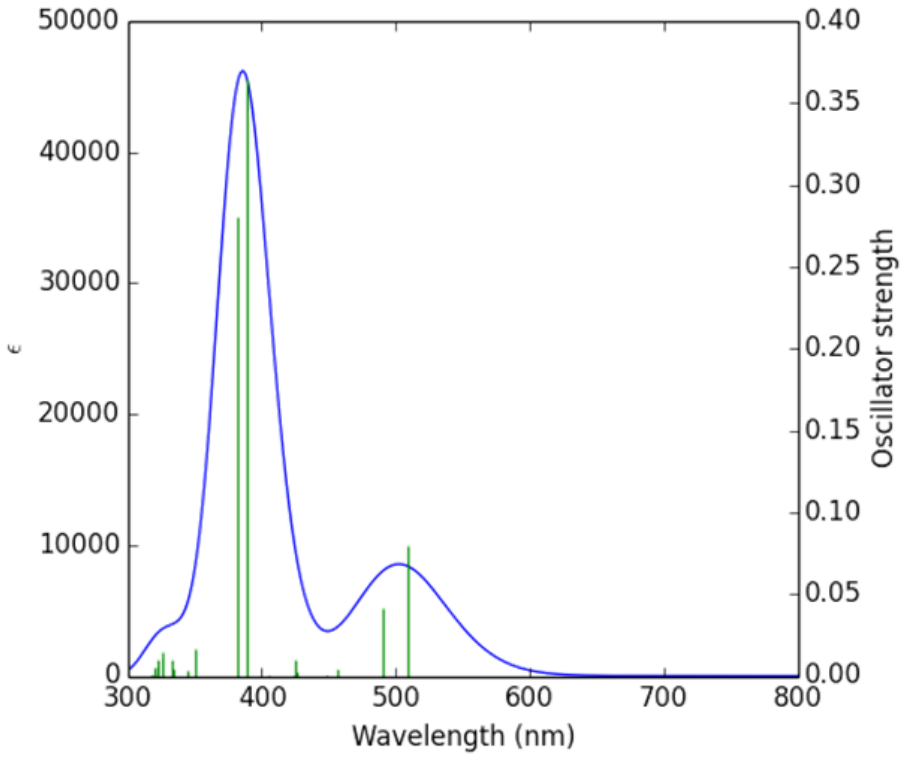

Figure S14. Calculated electronic absorption spectrum (UB3LYP/6-31G(d,p)) of **L1**.

Table S2. Selected TD-DFT (UB3LYP/6-31G(d,p)) calculated energies, oscillator strength and compositions of major electronic transitions of **L1**.

Wavelength (nm)	Osc. Strength	Symmetry	Major contribs
509.5	0.0794	2.148-A	H-2(β)->LUMO(β) (21%), HOMO(β)->LUMO(β) (69%)
490.7	0.0417	2.152-A	H-3(β)->LUMO(β) (27%), H-1(β)->LUMO(β) (64%)
456.5	0.0041	2.173-A	H-3(β)->LUMO(β) (54%), H-1(β)->LUMO(β) (31%)
448.6	0.0001	2.153-A	H-2(β)->LUMO(β) (64%), HOMO(β)->LUMO(β) (26%)
426.2	0.0028	2.119-A	H-5(β)->LUMO(β) (88%)
425.3	0.0097	2.098-A	H-4(β)->LUMO(β) (92%)
424.2	0.0003	2.130-A	H-6(β)->LUMO(β) (85%)
405.8	0.0001	2.298-A	H-7(β)->LUMO(β) (72%)
389.1	0.3648	2.344-A	HOMO(α)->LUMO(α) (68%), H-2(β)->LUMO(β) (11%)
381.5	0.2807	2.343-A	HOMO(α)->L+1(α) (68%), H-3(β)->LUMO(β) (10%)
350.7	0.0169	2.220-A	HOMO(α)->L+2(α) (91%)
344.1	0.0029	3.255-A	H-7(β)->LUMO(β) (13%)
334.1	0.0047	2.386-A	HOMO(α)->L+4(α) (81%)
332.5	0.0097	2.357-A	HOMO(α)->L+3(α) (81%)
326.4	0.0145	3.170-A	H-2(α)->LUMO(α) (13%), H-1(β)->L+1(β) (13%)
322.9	0.0099	3.260-A	H-1(α)->LUMO(α) (11%)
320.3	0.001	3.303-A	H-7(A)->L+2(α) (5%), H-5(β)->L+3(β) (5%), H-1(β)->L+1(β) (7%)
320.3	0.0051	3.328-A	H-6(α)->L+2(α) (6%), H-5(α)->L+3(α) (6%)
317.8	0.0009	2.129-A	H-8(β)->LUMO(β) (95%)
317.8	0.0007	2.097-A	H-9(β)->LUMO(β) (97%)

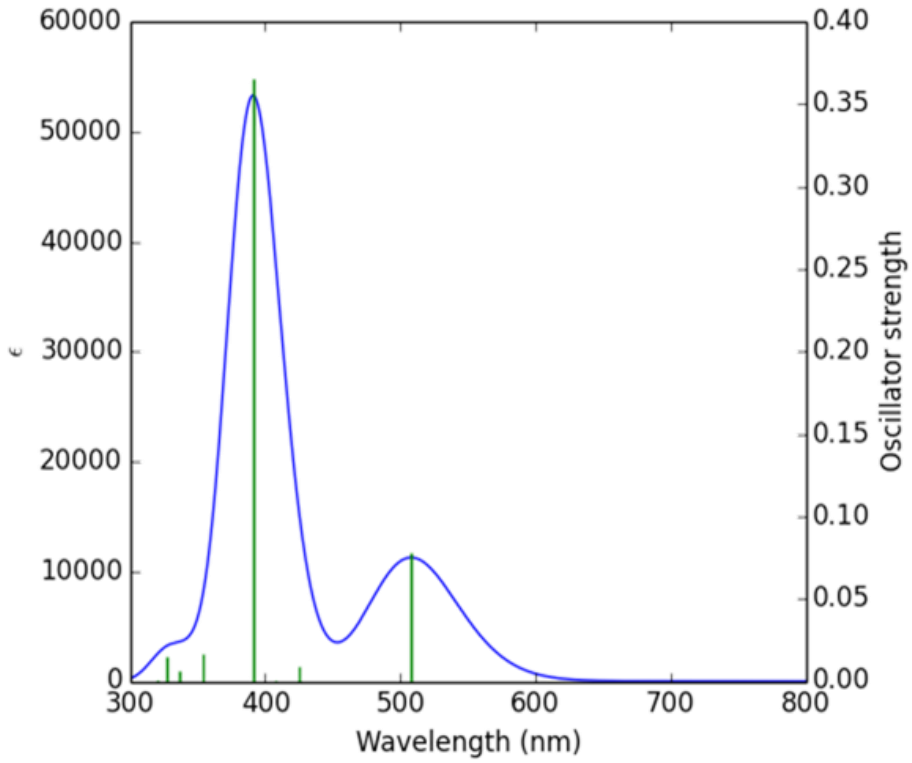

Figure S15. Calculated electronic absorption spectrum (UB3LYP/6-31G(d,p)) of **L2**.

Table S3. Selected TD-DFT (UB3LYP/6-31G(d,p)) calculated energies, oscillator strength and compositions of major electronic transitions of **L2**.

Wavelength (nm)	Osc. Strength	Symmetry	Major contribs
508.1	0.0777	2.149-A	H-3(β)->LUMO(β) (22%), HOMO(β)->LUMO(β) (69%)
508.0	0.0775	2.149-A	H-4(β)->LUMO(β) (22%), H-1(β)->LUMO(β) (69%)
474.9	0	2.124-A	H-2(β)->LUMO(β) (93%)
447.8	0	2.156-A	H-3(β)->LUMO(β) (62%), HOMO(β)->LUMO(β) (27%)
447.7	0	2.156-A	H-4(β)->LUMO(β) (62%), H-1(β)->LUMO(β) (27%)
425.5	0.009	2.098-A	H-5(β)->LUMO(β) (94%)
424.6	0.0005	2.128-A	H-7(β)->LUMO(β) (35%), H-6(β)->LUMO(β) (52%)
424.6	0.0005	2.128-A	H-7(β)->LUMO(β) (52%), H-6(β)->LUMO(β) (35%)
407.7	0.0001	2.274-A	H-8(β)->LUMO(β) (75%)
391.1	0.3649	2.319-A	HOMO(α)->LUMO(α) (68%), H-4(β)->LUMO(β) (11%)
391.0	0.3659	2.319-A	HOMO(α)->L+1(α) (68%), H-3(β)->LUMO(β) (11%)
353.8	0.0172	2.219-A	HOMO(α)->L+2(α) (91%)
347.8	0	3.287-A	H-8(β)->LUMO(β) (12%)
336.3	0.0065	2.380-A	HOMO(α)->L+3(α) (81%)
336.3	0.0064	2.380-A	HOMO(α)->L+4(α) (81%)
327.3	0.0144	3.184-A	HOMO(α)->LUMO(α) (8%), H-2(β)->L+1(β) (7%)
327.3	0.0144	3.184-A	H-3(α)->L+1(α) (7%), HOMO(α)->L+1(α) (8%), H-2(β)->L+2(β) (7%)
321.3	0	3.408-A	H-2(α)->LUMO(α) (10%), H-1(α)->L+1(α) (10%)
320.5	0.0009	3.327-A	H-7(α)->L+2(α) (6%), H-3(α)->LUMO(α) (8%)
320.5	0.0008	3.326-A	H-8(α)->L+2(α) (6%), H-3(α)->L+1(α) (8%)

2.2. Electronic and magnetic properties of the Co(II) ions in the complexes

The electronic structures and magnetic properties of the Co(II) ions in the coordination polymers **CoCP-1** and **CoCP-2** were first studied by using suitable single-Co fragment models **Co-1** and **Co-2** by using somewhat reduced ligands (Figure S14). All calculations were carried out with OpenMolcas version 18.0 and are of CASSCF/RASSI/SINGLE_ANISO type.[4]

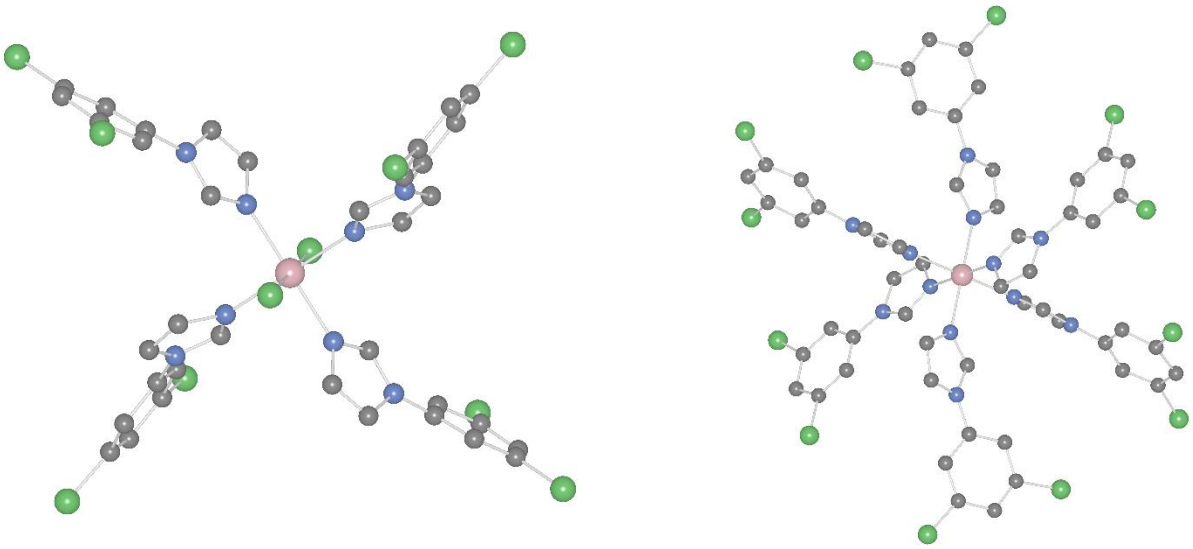

Figure S16. Structures using in CASSCF/RASSI/SINGLE_ANISO calculations of **Co-1** and **Co-2** complexes. Color scheme: Co – pink, N – blue and C – grey. Hydrogen atoms are omitted for clarity.

Three basis set approximations have been employed: **1** – small, **2** – medium, **3** – large. Table S4 shows the contractions of the employed basis sets for all elements.

Table S4. Contractions of the employed basis sets in computational approximations **1, 2** and **3**.

Basis 1	Basis 2	Basis
CO.ANO-RCC...4S3P1D	CO.ANO-RCC...5S4P2D1F	CO.ANO-RCC...6S5P3D2F1G
CL.ANO-RCC...3S2P	CL.ANO-RCC...4S3P1D	CL.ANO-RCC...5S4P2D1F
N.ANO-RCC...2S1P	N.ANO-RCC...3S2P1D	N.ANO-RCC...4S3P2D1F
C.ANO-RCC...2S1P	C.ANO-RCC...3S2P1D	C.ANO-RCC...4S3P2D1F
H.ANO-RCC...1S	H.ANO-RCC...2S	H.ANO-RCC...2S1P

Two active spaces were designed for CASSCF calculations: 7 electrons in 5 orbitals (CAS(7,5)) and 7 electrons in 10 orbitals (CAS(7,10)). 10 quartet and 40 doublet states were mixed by spin-orbit coupling. On the basis of the resulting spin-orbital multiplets SINGLE_ANISO program computed local magnetic properties (*g*-tensors, magnetic axes, local magnetic susceptibility, etc.).

Electronic and magnetic properties of **Co-1**

Table S5. Energies of the lowest spin-free states (cm^{-1}) of **Co-1**.

Spin-free energies, cm^{-1}				
CAS(7,5)	CAS(7,5)	CAS(7,5)	CAS(7,10)	CAS(7,10)
Basis 1	Basis 2	Basis 3	Basis 2	Basis 3
0.0	0.0	0.0	0.0	0.0
352.9	561.1	520.8	613.8	551.7
558.3	579.7	536.3	629.6	561.8
6071.4	5385.1	5280.5	5861.0	5733.3
7994.2	7586.2	7551.7	8202.4	8158.0
8274.8	7804.0	7773.2	8426.9	8389.9

Table S6. Energies of the lowest spin-orbit coupling doublets (cm^{-1}) of **Co-1**.

Spin-orbit energies, cm^{-1}				
CAS(7,5)	CAS(7,5)	CAS(7,5)	CAS(7,10)	CAS(7,10)
Basis 1	Basis 2	Basis 3	Basis 2	Basis 3
0.0	0.0	0.0	0.0	0.0
0.0	0.0	0.0	0.0	0.0
208.0	203.2	211.1	178.5	191.0
208.0	203.2	211.1	178.5	191.0
517.4	659.0	633.4	676.2	634.1
517.4	659.0	633.4	676.2	634.1
862.3	1023.4	1004.7	1010.3	981.9
862.3	1023.4	1004.7	1010.3	981.9
1078.8	1126.2	1105.0	1106.8	1071.5
1078.8	1126.2	1105.0	1106.8	1071.5
1169.3	1259.4	1233.6	1243.7	1203.8
1169.3	1259.4	1233.6	1243.7	1203.8

Table S7. *g*-tensors of the lowest spin-orbit doublets of **Co-1**.

KD		CAS(7,5) Basis 1	CAS(7,5) Basis 2	CAS(7,5) Basis 3	CAS(7,10) Basis 2	CAS(7,10) Basis 3
1	g_X	5.2807	6.2115	6.2395	6.1364	6.1764
	g_Y	4.8406	4.4137	4.3964	4.3871	4.3636
	g_Z	2.8521	2.3391	2.3700	2.2712	2.3251
2	g_X	0.1379	0.5974	0.5934	0.6285	0.6301
	g_Y	0.2508	0.9635	1.0033	0.9000	0.9484
	g_Z	5.5120	5.4653	5.3805	5.5681	5.4595
3	g_X	3.9937	2.6546	2.6526	2.5800	2.5837
	g_Y	3.0772	2.9804	3.0220	2.8884	2.9595
	g_Z	2.0683	4.3551	4.1668	4.7056	4.4076
4	g_X	0.1755	0.0018	0.0208	0.1706	0.1450
	g_Y	0.4788	0.6258	0.5876	0.8037	0.6722
	g_Z	3.8801	3.5850	3.6384	3.2481	3.3191
5	g_X	2.8269	1.9708	1.9111	0.1945	0.1909
	g_Y	2.0948	1.1518	1.2489	0.7325	0.8801
	g_Z	0.7894	0.2723	0.2752	1.9147	1.7831
6	g_X	0.3152	0.4054	0.3609	0.5176	0.4509
	g_Y	0.3963	0.4612	0.4155	0.5542	0.4866
	g_Z	3.5157	3.3242	3.2872	3.4035	3.3542

Electronic and magnetic properties of **Co-2**

Table S8. Energies of the lowest spin-free states (cm^{-1}) of **Co-2**.

Spin-free energies, cm^{-1}				
CAS(7,5)	CAS(7,5)	CAS(7,5)	CAS(7,10)	CAS(7,10)

Basis 1	Basis 2	Basis 3	Basis 2	Basis 3
0.0	0.0	0.0	0.0	0.0
215.1	240.6	235.6	256.8	248.2
308.4	454.9	432.6	500.9	463.4
8217.3	7769.6	7746.5	8487.6	8464.8
8391.2	7908.3	7885.2	8640.6	8618.1
8416.3	8064.2	8026.8	8806.1	8762.6

Table S9. Energies of the lowest spin-orbit coupling doublets (cm^{-1}) of **Co-2**.

Spin-orbit energies, cm^{-1}				
CAS(7,5)	CAS(7,5)	CAS(7,5)	CAS(7,10)	CAS(7,10)
Basis 1	Basis 2	Basis 3	Basis 2	Basis 3
0.0	0.0	0.0	0.0	0.0
0.0	0.0	0.0	0.0	0.0
261.6	253.2	256.1	228.0	233.8
261.6	253.2	256.1	228.0	233.8
438.5	484.4	479.1	478.4	470.6
438.5	484.4	479.1	478.4	470.6
889.9	914.9	915.6	862.4	865.7
889.9	914.9	915.6	862.4	865.7
943.4	1043.5	1032.5	1018.0	1000.4
943.4	1043.5	1032.5	1018.0	1000.4
1052.5	1161.8	1149.6	1133.0	1114.4
1052.5	1161.8	1149.6	1133.0	1114.4

Table S10. *g*-tensors of the lowest spin-orbit doublets of **Co-2**.

KD		CAS(7,5) Basis 1	CAS(7,5) Basis 2	CAS(7,5) Basis 3	CAS(7,10) Basis 2	CAS(7,10) Basis 3
1	g_X	5.1560	3.1121	5.5306	2.9528	3.0218
	g_Y	4.6118	4.3492	4.3899	4.2274	4.3038
	g_Z	3.3117	5.5919	3.1507	5.7256	5.6161
2	g_X	0.0315	0.2023	0.1629	0.3471	0.2712
	g_Y	0.2934	0.6959	0.6365	0.8295	0.7257
	g_Z	4.8509	4.9573	4.9435	5.0288	5.0037
3	g_X	2.9457	3.1943	3.1215	3.4214	3.2965
	g_Y	2.6405	2.7725	2.7708	2.8737	2.8506
	g_Z	2.2677	1.9011	1.9643	1.7384	1.8500
4	g_X	0.0801	0.0003	0.0395	0.0786	0.0206
	g_Y	0.4481	0.2763	0.2634	0.2843	0.2606
	g_Z	2.8520	3.2441	3.2205	3.3156	3.2802
5	g_X	0.5902	0.4968	0.4955	0.5208	0.5140
	g_Y	0.8093	0.9316	0.9287	0.9837	0.9792
	g_Z	2.3663	3.6498	3.5307	3.9117	3.7070

6	g_X	0.5657	1.0723	1.0275	1.1546	1.0813
	g_Y	0.6737	1.2157	1.1674	1.3273	1.2425
	g_Z	3.0613	3.1400	3.1164	3.2405	3.2049

Table S11. DFT calculations of the energy gaps between the ground spin doublet and ground spin quartet. The spin quartet is found to be the ground state in for all Co fragments. Energies are given in cm^{-1}.

Model	$\Delta E = E_{S=1/2} - E_{S=3/2}$	
	B3LYP	ωB97M-V
Co-1	3725	4683
Co-2	3923	4942

2.3. Broken-symmetry DFT calculations on the Co(II)-radical complexes (Co-R)

The Broken-symmetry DFT calculations were carried out within ORCA 5.0.0, using the B3LYP functional and def2-TZVP basis sets.[5] The wavefunction was represented by an unrestricted Slater determinant. The relativistic effects were considered via DKH in the basis sets. The exchange interaction is considered by the phenomenological Heisenberg spin Hamiltonian:

$$\widehat{H} = -2J_{ij}S_iS_j$$

The Co(II) ions (S=3/2) were replaced with Mn(II) ions (S=5/2) for the {Co-R} and {Co-Co} exchange interactions to avoid near-degeneracy complications (Co^{2+} in our distorted octahedral environment has a 4T triply near-degenerate ground state, which is not suitable for singly determinant DFT method). Rescaling factor for {Co-R} is 5/3, while for {Co-Co} is 25/9.

Co(II) ions were replaced with diamagnetic Zn(II) ions for {R-R} exchange interaction.

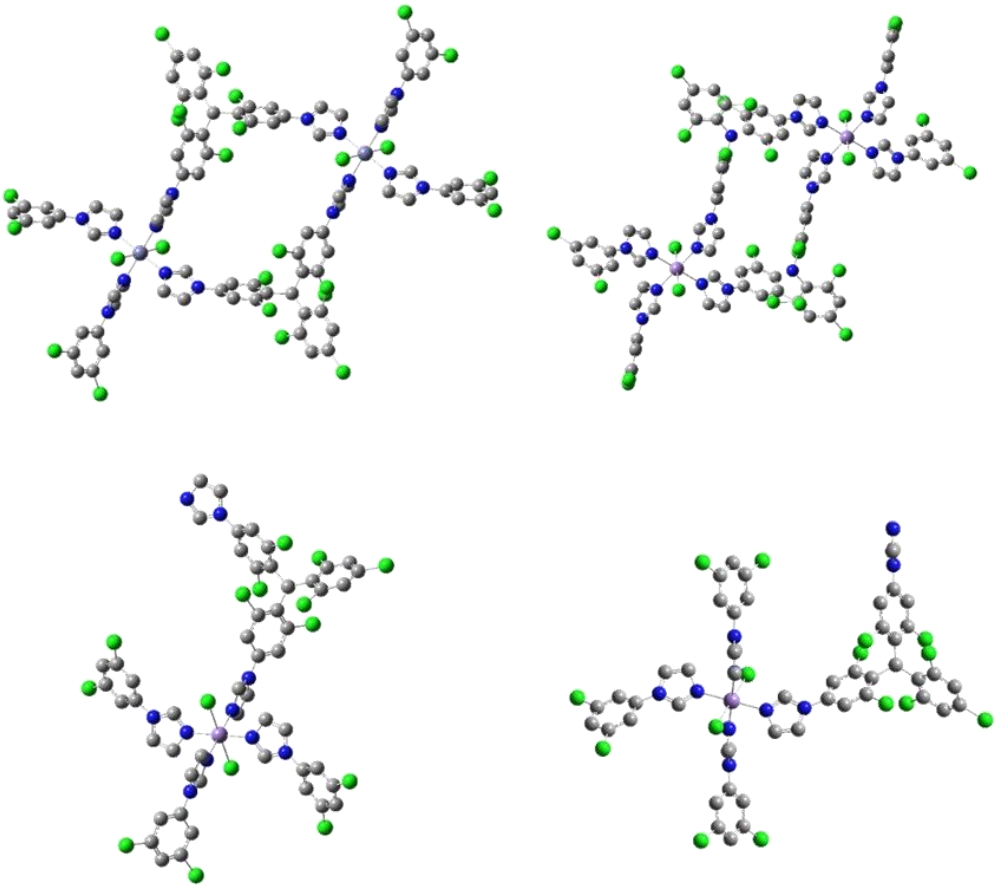

Figure S17. Structures using in BS-DFT calculations for **CoCP-1**. Top left: $J_{R1\text{-}R1}$, top right: $J_{Mn1\text{-}Mn2}$, bottom left: $J_{Mn1\text{-}R1}$, and bottom right: $J_{Mn1\text{-}R2}$. Color scheme: Zn – charcoal, Mn – pink, N – blue, C – grey and Cl – green. Hydrogen atoms are omitted for clarity.

The following results were obtained:

Table S12. Exchange parameters (cm^{-1}) of **CoCP-1**.

J_{ij}	Exchange obtained for Mn (S=5/2) fragments	Rescaled Exchange for Co (S=3/2)
$J_{R1\text{-}R1}$	0.10	0.10
$J_{Mn1\text{-}Mn2}$	0.04	0.11
$J_{Mn1\text{-}R1}$	-3.00	-5.00
$J_{Mn1\text{-}R2}$	-1.42	-2.37

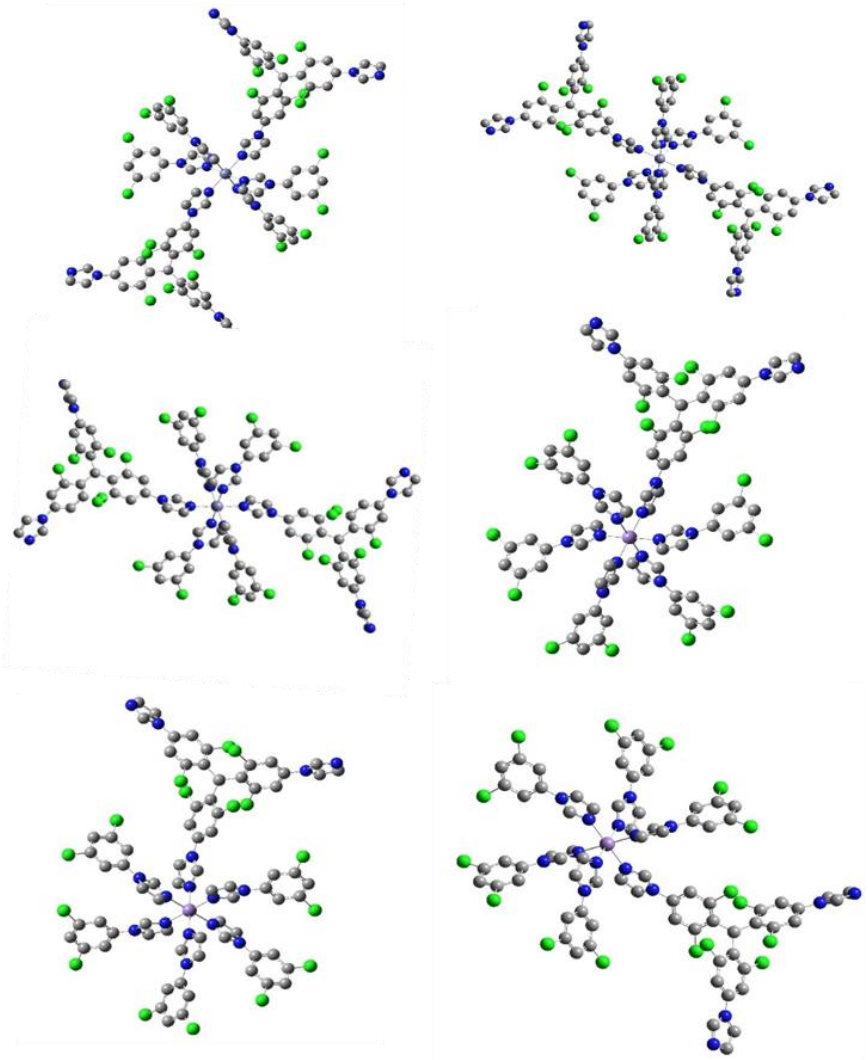

Figure S18. Structures using in BS-DFT calculations for **CoCP-2**. Top left: $J_{R1\text{-}R1}$, top right: $J_{R2\text{-}R2}$, middle left: $J_{R3\text{-}R3}$, middle right: $J_{Mn1\text{-}R1}$, bottom left: $J_{Mn1\text{-}R2}$, and bottom right: $J_{Mn1\text{-}R3}$. Color scheme: Zn – charcoal, Mn – pink, N – blue, C – grey and Cl – green. Hydrogen atoms are omitted for clarity.

Table S13. Exchange parameters (cm^{-1}) of **CoCP-2**.

J_{ij}	Exchange obtained for Mn (S=5/2) fragments	Rescaled Exchange for Co (S=3/2)
$J_{R1\text{-}R1}$	1.24	1.24
$J_{R2\text{-}R2}$	0.61	0.61
$J_{R3\text{-}R3}$	0.06	0.06
$J_{Mn1\text{-}R1}$	-1.33	-2.22
$J_{Mn1\text{-}R2}$	-1.84	-3.07
$J_{Mn1\text{-}R3}$	-2.04	-3.40

3. X-ray crystallography data

The crystal structures were solved by a direct method (SHELX-97[6]) and refined by full-matrix least-squares on F2 (SHELX-97[7]). The positions of non-hydrogen atoms were refined anisotropically. The hydrogen atoms were positioned geometrically and refined using a riding model, except for the guest molecules.

Table S14. Crystallographic data for **CoCP-1** and **CoCP-2**.

Identification code	**CoCP-1**	**CoCP-2**
Empirical formula	$C_{56}H_{38}Cl_{16}CoN_{10}O_2$	$C_{78}H_{72}Cl_{12}CoF_{12}N_{20}O_{14}S_4$
Formula weight	1509.09	2354.13
Temperature/K	100.0	100.00
Crystal system	triclinic	trigonal
Space group	P-1	R-3
a/Å	8.3433(5)	16.1717(7)
b/Å	15.7259(9)	16.1717(7)
c/Å	15.8421(9)	35.7861(12)
α/°	73.579(3)	90.00
β/°	79.914(3)	90.00
γ/°	87.343(3)	120.00
Volume/Å3	1963.0(2)	8105.1(6)
Z	1	3
ρcalcg/cm3	1.277	1.447
μ/mm-1	7.063	0.617
F(000)	759.0	3585.0
Crystal size/mm3	0.206 × 0.185 × 0.177	0.2 × 0.18 × 0.15
Radiation	CuKα (λ = 1.54178)	MoKα (λ = 0.71073)
2Θ range for data collection/°	5.858 to 133.68	5.04 to 50.04
Index ranges	-9 ⩽ h ⩽ 9, -18 ⩽ k ⩽ 18, -18 ⩽ l ⩽ 18	-19 ≤ h ≤ 19, -19 ≤ k ≤ 19, -42 ≤ l ≤ 42
Reflections collected	29413	54227
Independent reflections	6895 [Rint = 0.0848, Rsigma = 0.0688]	3188 [Rint = 0.1124, Rsigma = 0.0409]
Data/restraints/parameters	6895/0/387	3188/740/507
Goodness-of-fit on F2	1.059	1.159
Final R indexes [I>=2σ (I)]	R1 = 0.0801, wR2 = 0.2240	R1 = 0.0985, wR2 = 0.2203
Final R indexes [all data]	R1 = 0.0983, wR2 = 0.2357	R1 = 0.1111, wR2 = 0.2284
Largest diff. peak/hole / e Å-3	1.56/-2.2	0.73/-0.80

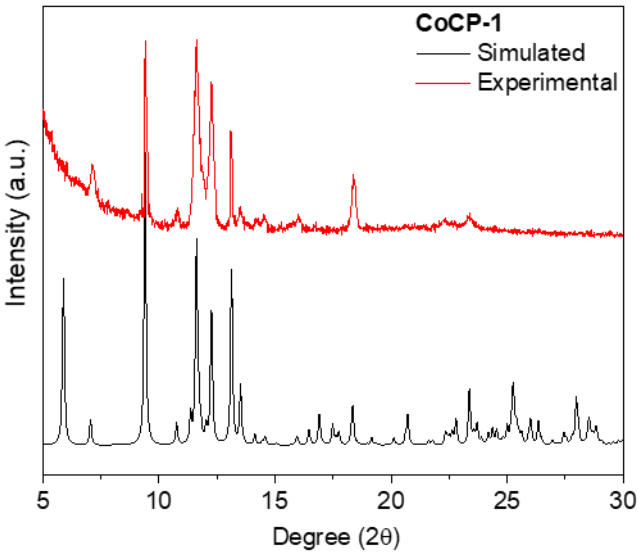

Figure S19. Experimental (red) and simulated (black) PXRD patterns for **CoCP-1**.

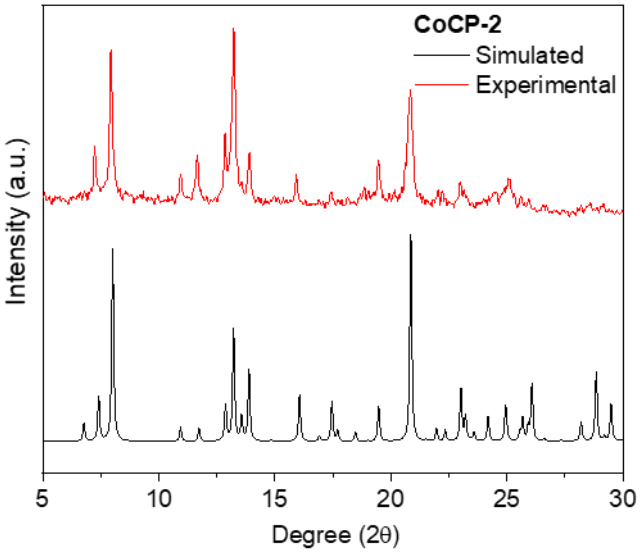

Figure S20. Experimental (red) and simulated (black) PXRD patterns for **CoCP-2**.

4. XPS and valence bond analysis

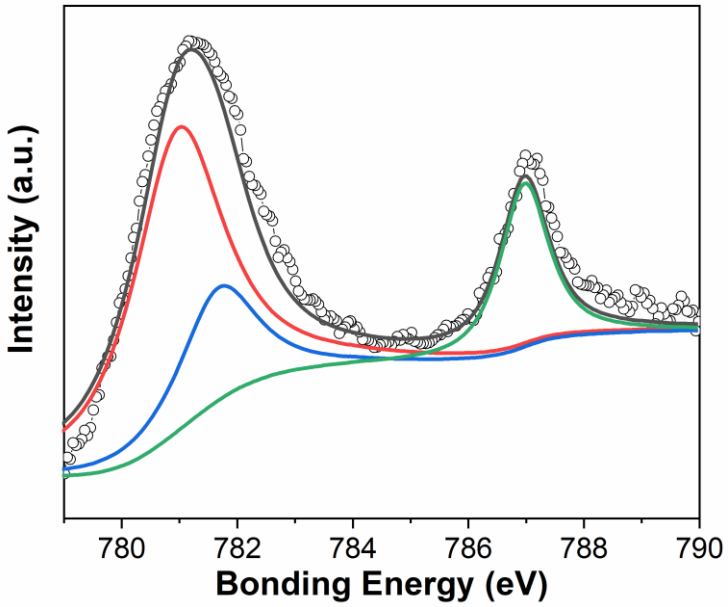

Figure S21. The XPS spectra of compound **CoCP-1** with Co 2p3/2. Measurement data (black open cycle), fitting data (black), simulated with peak 1 at 781 eV (red), simulated with peak 2 at 781.7 eV (blue), and simulated with peak 3 at 787.1 eV(green).

Table S15. Analytical data of XPS for **CoCP-1**

	Peak position （eV）	Width (eV)	Area
Co （2+）	781	2.28	3511.973
	787.1	1.03	1960.452
Co （3+）	781.7	1.60	834.575

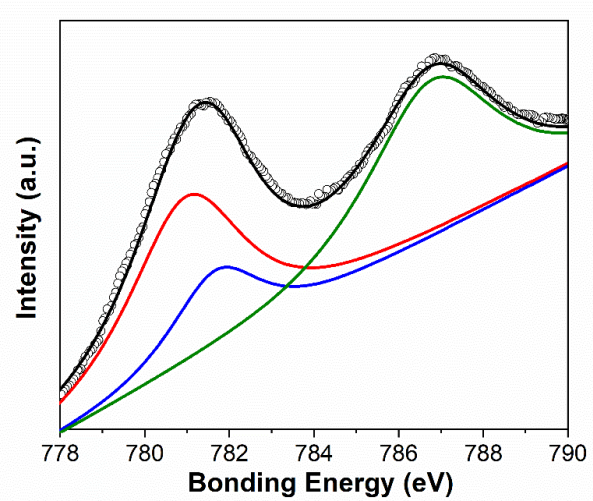

Figure S22. The XPS spectra of compound **CoCP-2** with Co 2p3/2. Measurement data (black open cycle), fitting data (black), simulated with peak 1 at 781 eV (red), simulated with peak 2 at 781.7 eV (blue), and simulated with peak 3 at 787.1 eV (green).

Table S16. Analytical data of XPS for **CoCP-2**

	Peak position（eV）	Width (eV)	Area
Co（2+）	781	3.26	3673.9681
	787.1	3.65	3771.4263
Co（3+）	781.7	3.06	1427.1089

Table S17. Valence bond for **CoCP-1** and **CoCP-2**

	CoCP-1	**CoCP-2**
Ratios of Co(II)/Co(III)(from XPS)	3.277	2.6082
Co-N dist(from SCXRD)	2.123(4)	2.152(3)
Valence bond	2.1487	2.3239

The Valence bond of Co from SCXRD data is calculated using the equation below.[8]

$$V_{ij} = e\,[\,(R_0 - d_{ij})/B\,]$$

$$V_i = \pm \sum j\, V_{ij}$$

R_0 =1.84, B=0.37, d_{ij} is the bond distance. In this situation, only six N atoms bond to Co.

The calculated Co valences from the band valence analysis for **CoCP-1** and **CoCP-2** are 2.1487 and 2.3239, respectively (Table S17) which agree with the XPS results which shows the ratio of Co(II)/Co(III) in **CoCP-1** is 3.277 and 2.6082 in **CoCP-2**. From the temperature-dependent molar magnetic susceptibility result of Figure 4 in the main text, the higher X_mT value of **CoCP-2** may be due to the higher component of Co(III) in **CoCP-2** than **CoCP-1**. Mixed-Valence cobalt (II/III) and carbon radicals in **CoCP-2** and **CoCP-1** will further influence each other, especially the spin-orbital coupling can influence the magnetic behavior.

5. $^{1}H/^{13}$ NMR and mass spectra of new compounds

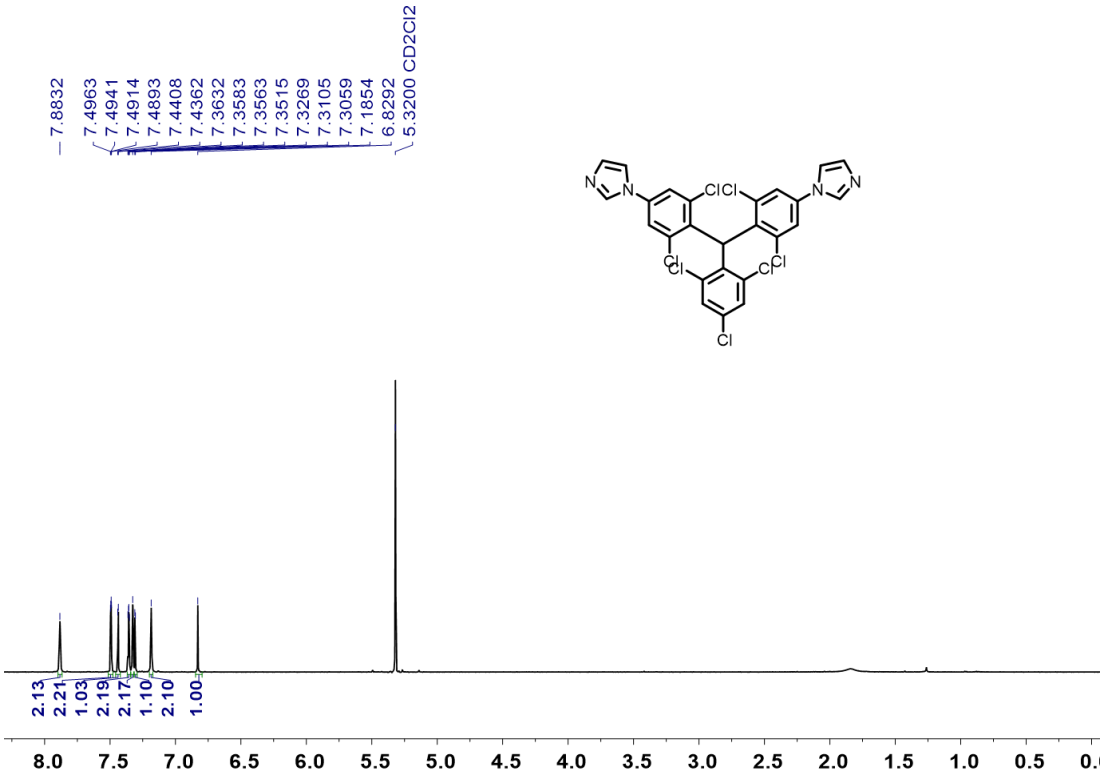

Figure S23. ^{1}H NMR spectrum (500 MHz, $CDCl_3$, 25 °C) of **L1-H**.

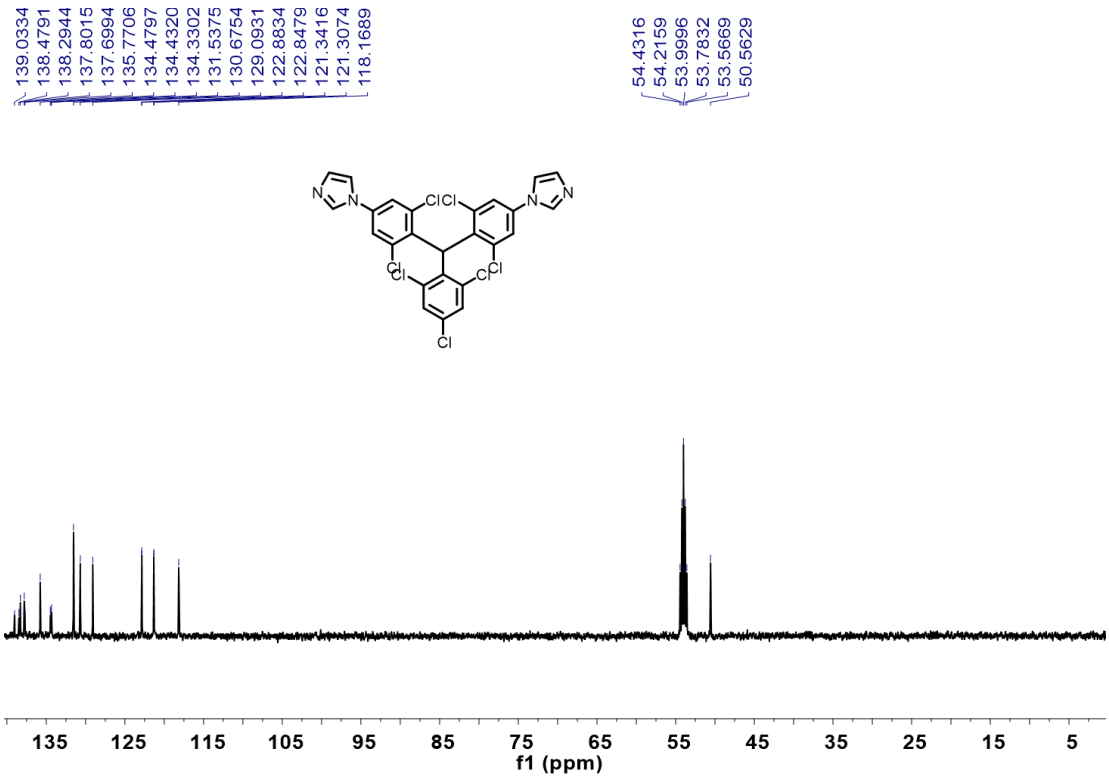

Figure S24. ^{13}C NMR spectrum (125 MHz, $CDCl_3$, 25 °C) of **L1-H**.

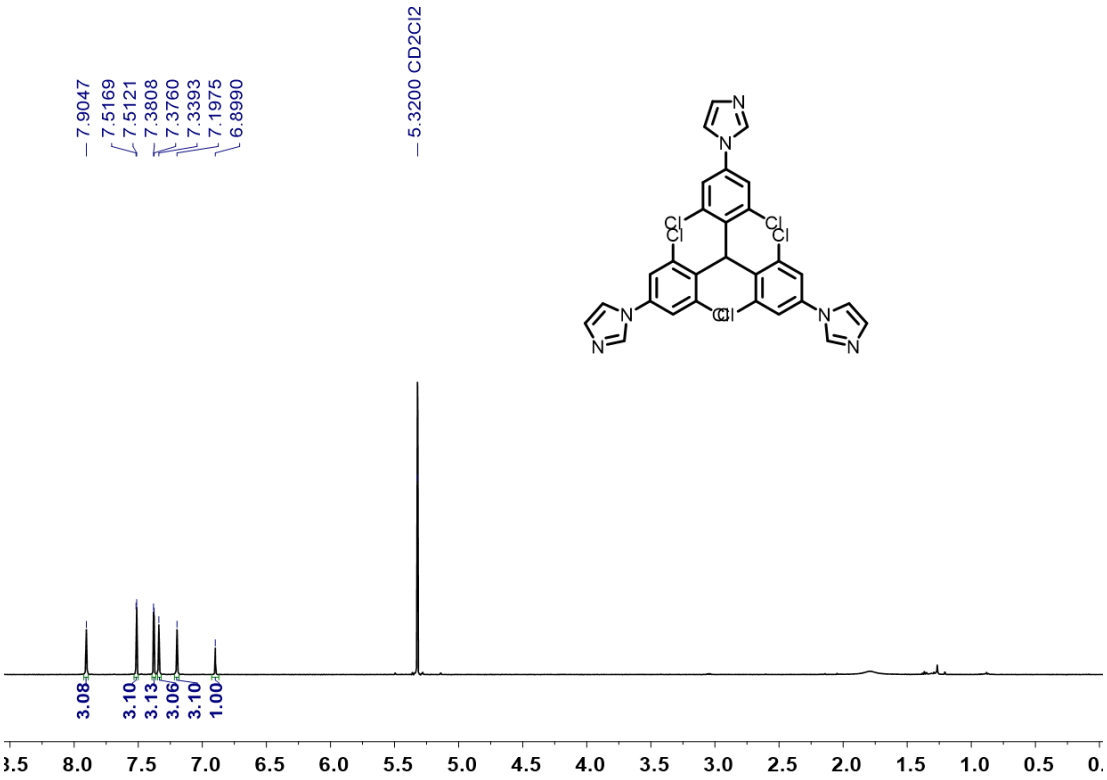

Figure S25. ^{1}H NMR spectrum (500 MHz, $CDCl_3$, 25 °C) of **L2-H**.

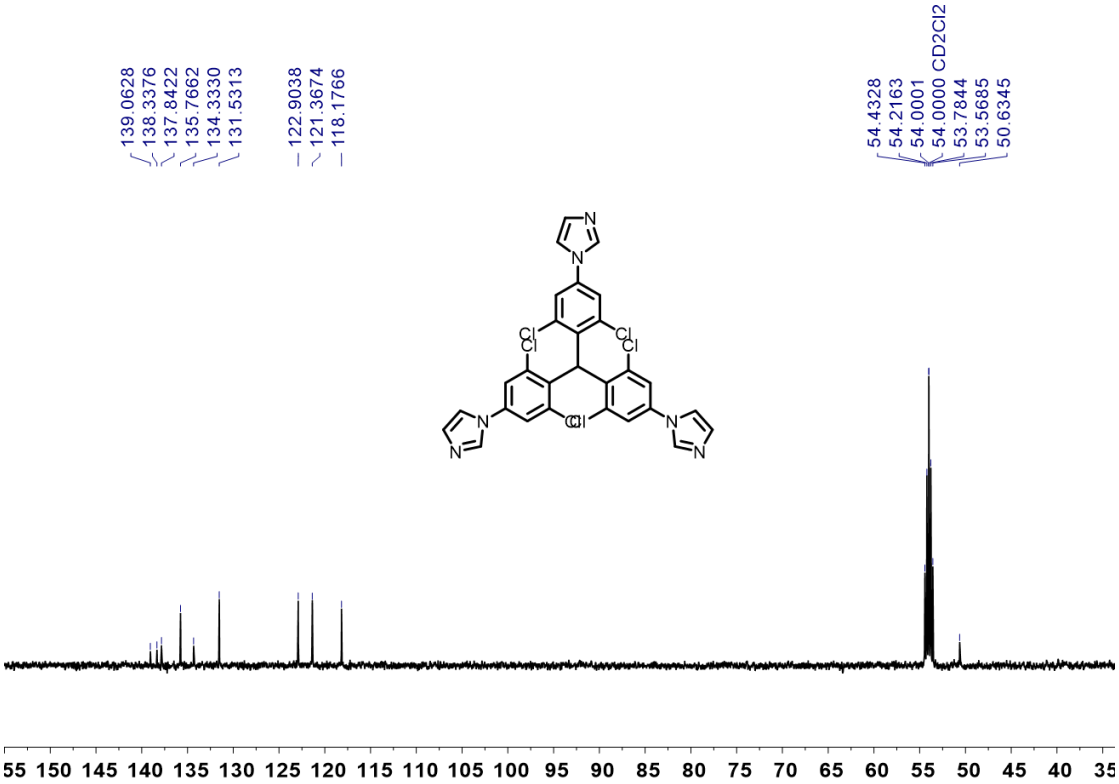

Figure S26. ^{13}C NMR spectrum (125 MHz, $CDCl_3$, 25 °C) of **L2-H**.

Meas. m/z	#	Formula	Calc. Mass	Err [ppm]
614.9038	1	C25 H14 Cl7 N4	614.9033	0.81

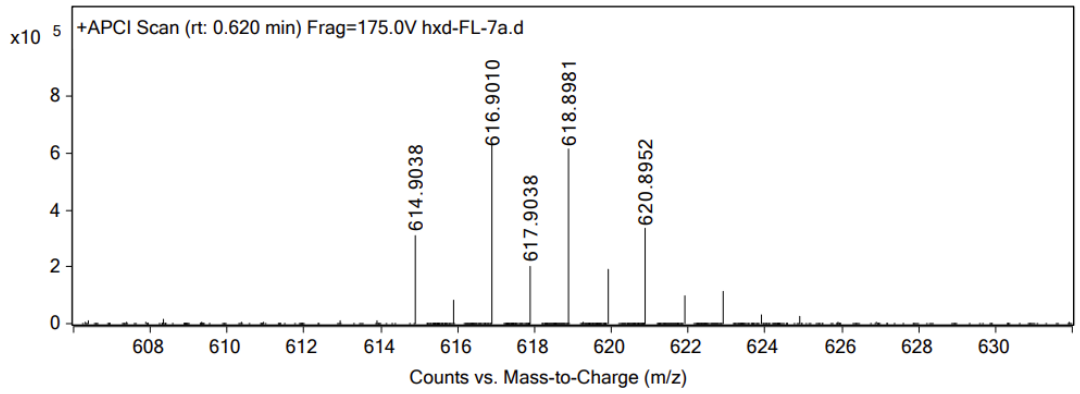

Figure S27. HR mass spectrum (APCI) of **L1-H**.

Meas. m/z	#	Formula	Calc. Mass	Err [ppm]
613.8959	1	C25 H13 Cl7 N4	613.8954	0.81

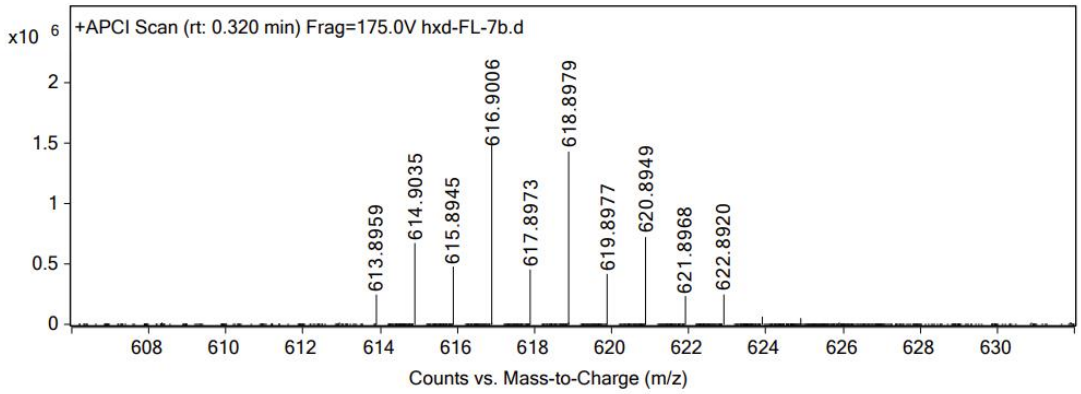

Figure S28. HR mass spectrum (APCI) of **L1**.

Meas. m/z	#	Formula	Calc. Mass	Err [ppm]
646.9644	1	C28 H17 Cl6 N6	646.964	0.62

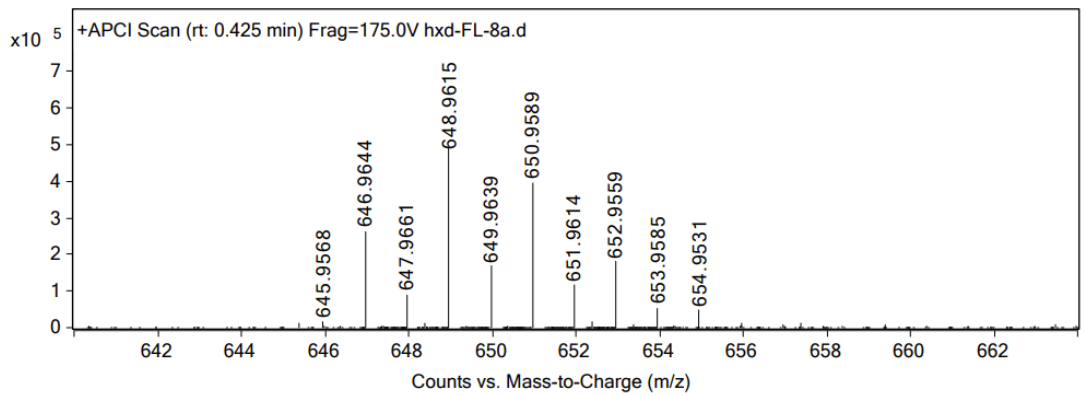

Figure S29. HR mass spectrum (APCI) of **L2-H**.

Meas. m/z	#	Formula	Calc. Mass	Err [ppm]
645.9571	1	C28 H16 Cl6 N6	645.9562	1.39

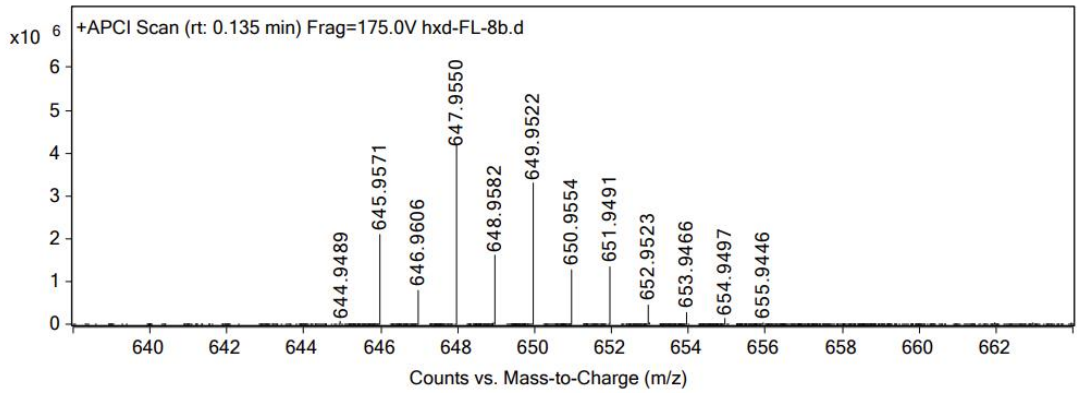

Figure S30. HR mass spectrum (APCI) of **L2**.

6. References

[1] O. Armet, J. Veciana, C. Rovira, J. Riera, J. Castaner, E. Molins, J. Rius, C. Miravitlles, S. Olivella, J. Brichfeus, *J. Phys.Chem.***1987**, *91*, 5608-5616.

[2] G. A. Bain and J. F. Berry, *J. Chem. Educ.* **2008**, *85*, 532-536.

[3] Gaussian 09; Revision A.2; Frisch, M. J.; Trucks, G. W.; Schlegel, H. B.; Scuseria, G. E.; Robb, M. A.; Cheeseman, J. R.; Scalmani, G.; Barone, V.; Mennucci, B.; Petersson, G. A.; Nakatsuji, H.; Caricato, M.; Li, X.; Hratchian, H. P.; Izmaylov, A. F.; Bloino, J.; Zheng, G.; Sonnenberg, J. L.; Hada, M.; Ehara, M.; Toyota, K.; Fukuda, R.; Hasegawa, J.; Ishida, M.; Nakajima, T.; Honda, Y.; Kitao, O.; Nakai, H.; Vreven, T.; Montgomery, J., J. A.; Peralta, J. E.; Ogliaro, F.; Bearpark, M.; Heyd, J. J.; Brothers, E.; Kudin, K. N.; Staroverov, V. N.; Kobayashi, R.; Normand, J.; Raghavachari, K.; Rendell, A.; Burant, J. C.; Iyengar, S. S.; Tomasi, J.; Cossi, M.; Rega, N.; Millam, N. J.; Klene, M.; Knox, J. E.; Cross, J. B.; Bakken, V.; Adamo, C.; Jaramillo, J.; Gomperts, R.; Stratmann, R. E.; Yazyev, O.; Austin, A. J.; Cammi, R.; Pomelli, C.; Ochterski, J. W.; Martin, R. L.; Morokuma, K.; Zakrzewski, V. G.; Voth, G. A.; Salvador, P.; Dannenberg, J. J.; Dapprich, S.; Daniels, A. D.; Farkas, Ö.; Foresman, J. B.; Ortiz, J. V.; Cioslowski, J.; Fox, D. J.; Gaussian, Inc., Wallingford CT, 2009.

[4] Fdez. Galván, I.; Vacher, M.; Alavi, A.; Angeli, C.; Aquilante, F.; Autschbach, J.; Bao, J. J.; Bokarev, S. I.; Bogdanov, N. A.; Carlson, R. K. Openmolcas: From source code to insight. *J. Chem. Theory Comput.* **2019**, *15*, 5925-5964

[5] F. Neese, *J. Phys. Chem. Solids* **2004**, *65*, 781-785.

[6] SHELXT-Integrated space-group and crystal-structure determination Sheldrick, G. M. *Acta Crystallogr., Sect. A* 2015, A71, 3.

[7] SHELXTL G. M. Sheldrick, Ver. 2014/7. *Acta Crystallographica. Sect C Structural Chemistry* 71, 3-8.

[8] Zhang, J., Ouyang, J., Ye, Y., Li, Z., Lin, Q., Chen, T., Xiang, S. *ACS applied materials & interfaces* **2018**, *32*, 27465-27471.